CFD MODELLING OF THE CIRCE FACILITY

K. Zwijsen*, D. Dovizio*, V. Moreau° and F. Roelofs*

* NRG, Westerduinweg 3, Petten, Netherlands
°CRS4, Science and Technology Park Polaris – Piscina Manna, 09010 Pula, Italy

ABSTRACT
CIRCE is a test facility designed and realized by the Italian agency ENEA to support the heavy liquid metal technology for nuclear fission plants. Within the H2020 projects SESAME and MYRTE, various experiments are performed in this facility, using two different heat exchangers (namely ICE and HERO), resembling nominal operation and accident scenarios of a Liquid Metal Fast Reactor (LMFR). Simultaneously, within this project different thermal-hydraulics models of CIRCE are created to gain experience in the modelling of such a facility and to help future development of LMFRs. At NRG and CRS4, CFD models of CIRCE in the two different configurations are created. The present paper describes the steps taken to create these models. Results obtained with the models are, where possible, compared with experimental results, both for steady-state and transient conditions. For the steady-states, generally good agreement is found. The main features of the stratification forming in the pool are recovered, though they appear quite sensitive to the local heat balance. The transient simulation performed recovers some of the main features of the experiment, however excessive cooling is found. The causes of discrepancies found between numerical and experimental results are currently under investigation.

1. INTRODUCTION

The behaviour of the coolant is an integral part in the safe operation of nuclear power plants, with its main function being the removal of the heat generated by the nuclear fission processes to secondary systems. During nominal operation of the reactor, this behaviour is pretty well established. However, in emergency situations, such as pump or heat exchanger failure, this is much less known, while it could significantly impact the nuclear reactor's functioning. For example, recirculation of the coolant could lead to temperatures increasing beyond safety thresholds, potentially giving rise to drastic events.

Experimental analysis on the coolant's flow and thermal behaviour is very challenging, if not impossible. Therefore, more and more is relied on computational thermal-hydraulics to provide insights on flow patterns and temperature distributions of the coolant. Initially, computational thermal-hydraulics analysis of nuclear reactors was either limited to very simplified models for the full system, or to more accurate models of only parts of the reactor, such as the rod bundle or the heat exchanger. However, with the increase in computer power and capacity, and the advancements being made in numerical modelling, it is now possible to resolve the full flow and thermal fields of the reactor on a, relatively, fine and detailed scale, using Computational Fluid Dynamics (CFD).

This paper focusses on the modelling of the main pool of Liquid Metal Fast Reactors (LMFRs) using CFD tools. In contrary to the common Light Water Reactors (LWRs), such as Boiling Water Reactors (BWRs) and Pressurized Water Reactors (PWRs), these Gen IV type reactors use liquid metals, such as pure lead, sodium or Lead-Bismuth Eutectic (LBE), as coolant. These liquid metals behave quite differently than light water, among others due to their much higher densities and thermal conductivities. Furthermore, their higher boiling temperatures allow the reactor to operate at much higher temperatures, which allows LMFRs to be more efficient.

The main aspects in pool modelling are discussed through the modelling of the Italian CIRColazione Eutettico (CIRCE) heavy liquid-metal pool-type facility, which uses LBE as coolant (Bandini et al., 2011 & Tarantino et al., 2015). Initially, as part of the European Horizon 2020 projects called SESAME (thermal hydraulics Simulations and Experiments for the Safety Assessment of MEtal cooled reactors), the CIRCE facility was operated in its Integral Circulation Experiments (ICE) set-up (Tarantino and Scaddozzo, 2006 & Tarantino, 2013) . Two different CFD models of this facility are created and discussed in this paper. The first one is NRG's Fluent model, with the second one being CRS4's StarCCM+ model. The different modelling strategies are presented, as well as several results for steady-state conditions. A transient test case representing a Protected Loss Of Heat sink and Loss Of Flow (PLOH + LOF) accident scenario is also performed using NRG's model. Numerical results are, where possible, compared with experimental data obtained from the CIRCE facility.

For the current, on-going, experimental campaign of CIRCE, the heat exchanger is replaced by a new one called HERO (Heavy liquid mEtal – pRessurized water cOoled tube, Rozzia et al. (2016), Pesetti et al. (2018a)). Both CFD models are subsequently adjusted to take this modification, as well as the different operational settings, into account. Steady-state simulations using both models are performed and compared whenever possible to experimental data obtained during the European Horizon 2020 project MYRTE (MYRRHA Research and Transmutation Endeavour).

2. CIRCE FACILITY

The CIRCE facility, including the ICE and HERO test sections, have been described extensively in previous reports (Tarantino (2013), Pesetti et al. (2018a)). It will be repeated here only briefly, highlighting the main components and the LBE flow loop.

2.1 CIRCE-ICE

The CIRCE facility, including the ICE test section, is depicted in Figures 1 (left) and 2. It consists of an inner loop and a main pool. The LBE enters the inner loop through a feeding conduit, after which it flows through a flow meter before entering the Fuel Pin Simulator (FPS). The FPS is a mechanical structure representing the heat source of the system. After exiting the FPS, the LBE passes through the fitting volume and flows inside the riser. Inside the riser there is a nozzle installed to allow argon injection, which forces the flow upwards. The LBE subsequently enters the separator, which is open from the top and allows for the separation of the argon, which flows into the cover gas through the free surface, and the LBE, which goes downward into the heat exchanger, where it gets cooled and re-enters the main pool. Finally, a Decay Heat Removal (DHR) system is installed that serves as heat exchanger in accident scenarios in which the primary heat exchanger stops working. Chapter 3 contains more details on several components.

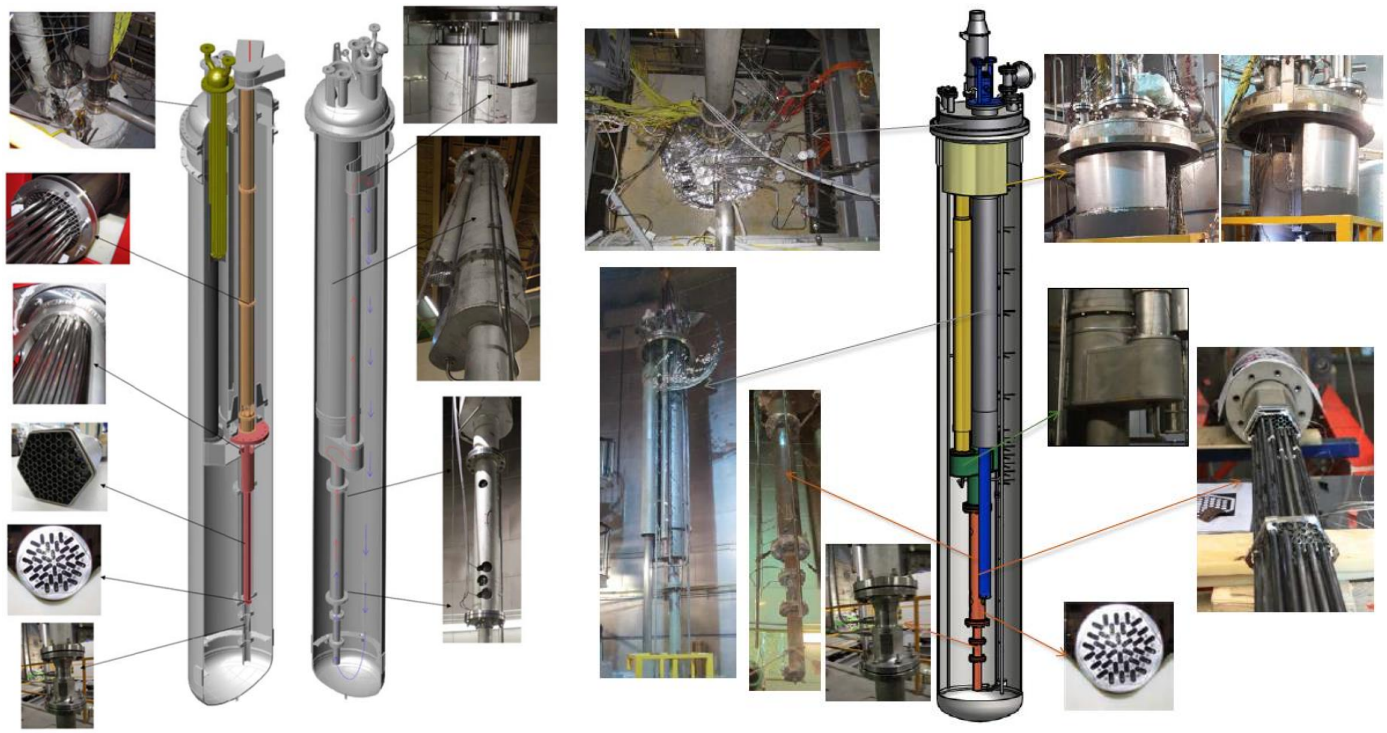

Figure 1: CIRCE facility in its ICE (left, Tarantino (2013)) and HERO (right, Pesetti et al. (2018)) configuration.

2.2 CIRCE-HERO

Upon completion of the experimental campaign of CIRCE-ICE, its heat exchanger was replaced by a thinner, longer one named HERO (Pesetti et al. (2018a)). This heat exchanger is a mock-up of the heat exchanger to be used in the Belgium multifunctional reactor MYRRHA (Multi-purpose hYbrid Research Reactor for High-tech Applications) and can be seen in Figure 1 (blue cylinder in the right CAD image). HERO is installed inside the outer shell of the ICE heat exchanger (grey cylinder in CAD image on the right), with all other parts of the CIRCE-ICE heat exchanger removed. More details on HERO can be found in Chapter 8. As HERO also serves as a DHR system in accident scenario tests, the DHR that is present in the CIRCE-ICE test section has been removed completely for experiments inside the CIRCE-HERO test facility. No further changes are made to the test facility when switching from the ICE configuration to the HERO configuration, meaning the flow path of LBE is the same as before. Additional thermocouples were installed though to better characterise the system.

3. NRG'S CIRCE-ICE MODEL USING ANSYS FLUENT

This chapter gives a detailed description of the CFD model of CIRCE-ICE created by NRG using ANSYS Fluent.

3.1 CAD Geometry

In the right of figure 2, the CAD geometry used for the simulations presented in this report is shown, along with arrows indicating how various parts of the actual test facility are represented. One of the major simplifications made is modelling the test section

between the feeding conduit and the fitting volume, which also includes the flow meter and the FPS, as one long cylinder with a constant radius. Furthermore, no bolts, flanges, etc. are included in the CAD geometry, and almost all walls have zero thickness, the exception being the heat exchanger wall. Also, the top lid is not included in the geometry. As a matter of fact, the CAD geometry only extends up till the free surface, so no cover gas is present in the model. In the sections below, several parts are discussed in detail.

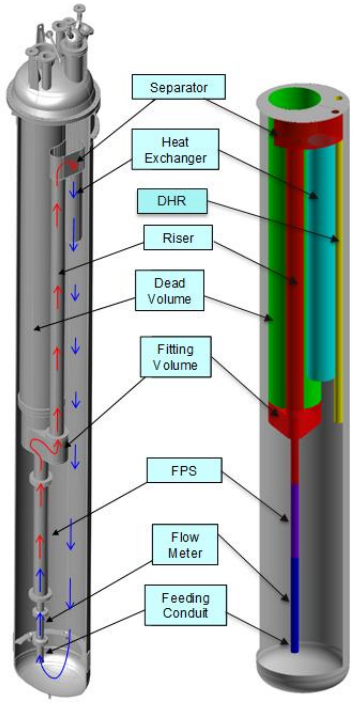

Figure 2: NRG's CAD geometry of CIRCE-ICE alongside test-facility.

3.2 Fuel Pin Simulator

The FPS consists of 37 electrical pins that heat the LBE. These pins have an active length of 1m (purple section in Figure 1) and extend all the way through the inner loop till the dead volume, where they are attached to electrical wires. No LBE is present inside this well-insulated dead volume. The pins are not physically present in the CAD model, but thermally accounted for by means of a constant Volumetric Heat Source (VHS) Q_{FPS}:

$$Q_{FPS} = \frac{P_{FPS}}{V_{FPS}}, \qquad (1)$$

where P_{FPS} is the desired power input and V_{FPS} the volume of the FPS section.

The flow resistance resulting from the electrical pins is modelled by treating the FPS as Porous Medium Zone (PMZ). Porous media are modelled by the addition of a momentum source term to the standard fluid flow equations. For the case of an homogeneous porous medium, which is applicable here, the source term reads:

$$S_i = -\left(\frac{\mu}{\alpha} v_i + C_2 \frac{1}{2} \rho |v| v_i\right) = \frac{\Delta p_{porous}}{L_{ref}}. \qquad (2)$$

Here, S_i is the source term for the i-th momentum equation, α the permeability and C_2 is the inertial resistance factor. In the current simulations the viscous losses (first term inside the brackets) are negligibly small compared with the inertial resistance term (second term inside brackets). From Equation (2), the inertial resistance coefficient can be determined if the pressure losses Δp_{porous} over the reference length L_{ref} are known:

$$C_2 = \frac{\Delta p_{porous}}{L_{ref} \frac{\rho}{2} \tilde{u}^2}, \qquad (3)$$

with $\tilde{u}$ the velocity of the LBE if the medium was fully open (superficial velocity).

To determine the pressure drop over the FPS cylinder, known friction coefficient correlations are used based on flow and thermal conditions relevant for the particular test scenario. The inertial resistance factor for flow in directions perpendicular to the main axial flow is set to a very large value, as in reality the pins restrict radial flow.

3.3 Argon Injection & Free Surface

To avoid the computational cost and complexity of a two-phase flow modelling approach, the argon injection, similar to a pumping mechanism, is not included explicitly, but modelled as a Volumetric Momentum Source (VMS) in the riser, much like what is used to model the heat input in the FPS. Furthermore, the model only extends up till the free surface, as no argon-LBE separation is needed. This free surface is modelled as an impenetrable wall with free-slip condition and is maintained at a fixed height, with the height based on the level of LBE observed during experiments. It should be noted that this height depends on the temperature of the LBE, so it does vary between experiments, albeit marginally.

3.4 Heat Exchanger

The primary heat exchanger in the CIRCE-ICE test facility is a low-pressure boiling water shell heat exchanger consisting of 91 bayonet tubes (Tarantino (2013)), as shown in Figure 3. Since the main interest is the heat being removed by the heat exchanger and the resulting temperature profile, and not so much the details of the flow field inside the heat exchanger, the tubes are not explicitly included in the geometry. To compensate for the friction losses due to the bayonet tubes, the heat exchanger is also modelled as a porous medium, using the same equation as is used for the FPS, i.e., Equation (2). The pressure loss due to friction are estimated using the Churchill correlation (Todreas and Kazimi (1993)).

A VHS is used again to model the thermal behavior. However, opposed to the FPS where a uniform model is used, the HX uses a model that depends on the local temperature according to:

$$Q_{HX} = \frac{\rho c_p}{\tau}(T_0 - T), \qquad (4)$$

here, ρ is the density of the LBE, c_p the specific heat, T the calculated temperature of the LBE, T_0 a target temperature and τ is a relaxation time. Such a model introduces two additional degrees of freedom, T_0 and τ, which allows for a better control over the temperature in the simulation: An increase in temperature in the system is met with a stronger heat sink. The parameters T_0 and τ are chosen based on the heat extracted by the heat exchanger during the simulated experiments.

Figure 3: View of the ICE HX installed into the test section.

In case of accident scenarios, in which the primary heat exchanger is no longer operational, the DHR serves as the heat sink of the system. It consists of a single bayonet tube, with LBE flowing in through slots from the top and leaving at the bottom. As the secondary side of the DHR is not included in the model, only the annular cylinder through which the LBE flows is incorporated in the model. A relation similar to Equation (4) is used to specify the amount of heat removed by the DHR.

3.5 Conjugate Heat Transfer

One of the more important phenomena taking place during the operation of the test facility is Conjugate Heat Transfer (CHT). This contributes to the heat balance of the system in two ways: 1) heat transfer from the hot inner loop to the colder main pool through the inner structures, e.g., through the fitting volume walls, and 2) heat transferred from the main pool to the environment through the vessel walls, and, to a lesser degree, through the dead volume walls. In order to get an accurate model, and to get a proper stratification in the pool, CHT should not be neglected.

In the NRG model, in which almost all the walls have zero physical thickness, the Shell Conduction option of Fluent is used. This option allows to create additional layers of cells in walls, in which, during the simulation, the heat equation is solved. This Shell Conduction option requires the specification of the thickness of the layer as well as the material, and takes into account heat transfer through the walls, as well as in-wall heat conduction and thermal inertia of the walls. The latter is important during transient runs, when heat contained in the walls slows down the cooling of the system.

4. CRS4'S CIRCE-ICE MODEL USING STAR-CCM+

CRS4's CFD model of CIRCE-ICE is created using STAR-CCM+. It is described in detail in this chapter.

4.1 CAD Geometry

The CAD geometry used in CRS4's Star-CCM+ model of CIRCE-ICE can be seen in the left of Figure 4, which also include close-ups of several structural parts. As it is anticipated that a high level of detail is necessary for the representation of the local flow patterns in the plenum that strongly influence the various walls heat flux, a particular effort has been done to have a quite detailed numerical geometry. The full test facility is modelled, including the cover, all internal structures and all structural walls. Flanges and holes used for instrumentation are also included, though screws and bolts are considered too much detail and hence are ignored. The modelling of several important parts is discussed in detail in the next sections.

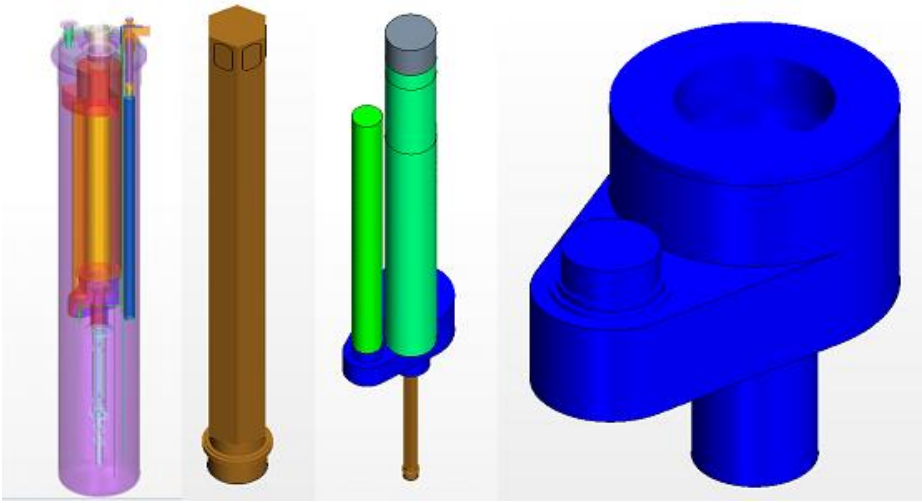

Figure 4: CRS4's CAD geometry alongside several isolated structural parts.

4.2 Fuel Pin Simulator

The electrical pins that heat the LBE are not included in the CAD geometry. A heat source is added to the CFD model to represent the pins' thermal power. Initially, a constant density heat source localised inside a numerical hexagonal region surrounding and overlapping the active part of the pin bundle was used. However, measurements taken at the top of the FPS active part indicate a strong decrease of the temperature from the centre to the periphery of the bundle. Extrapolating roughly from these incomplete data, it is quite probable that the external wall temperature remains essentially close to the FPS inlet temperature and that the conjugate heat transfer towards the plenum is quite limited. To reproduce qualitatively this effect, the heat source is restricted to a cylindrical region slightly smaller than the hexagonal geometry, such as to stay a little away from the external wall. Figure 5 illustrates this heat source, along with its effect on the temperature field inside the FPS.

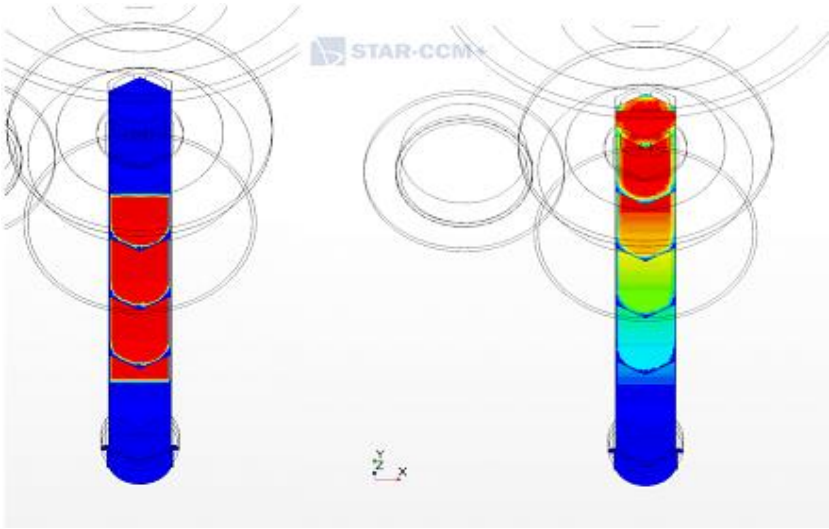

Figure 5: shape of the heat source in the model FPS region (left) and corresponding temperature profile (right).

Regarding the hydraulic resistance caused by the pins, this is accounted for in the model by means of a porous medium.

4.3 Riser with Argon Injection

Feasibilities studies were performed to include forcing of the flow by means of argon injection in the model. Even though successfully implemented, it resulted in excessively long computational time due to the very small size of the nozzle and the very high velocity the flow should reach there. Replacing it by buoyant Lagrangian particles did not necessarily resolve these problems. Since it is hard to evaluate if and how much either the argon injection or the Lagrangian particles would improve the model, it is decided to model the forcing simply by a vertical momentum source.

Preliminary tests showed that there was a discrepancy between the model's riser temperature outlet and that coming from the experiments; the model one was quite a bit lower. A possible cause is the presence on the riser walls of a layer LBE oxide, which has a low thermal conductivity. Therefore, an extra thermal resistance to the corresponding fluid-solid interface was added to the model.

4.4 Separator Bypass Flow

It is plausible that some LBE passes directly from the separator to the main pool through splashing at the riser outlet and/or due to a leakage at the separator-riser connection. The amount is however totally unknown. The numerical model is unable to simulate directly the droplet ejection, while the leakage would require a rather complicated modification of the geometry. To obtain a similar effect though in the model, some LBE disappears from the gas separator and directly reappears at the plenum top. Numerically, this is done by (i) setting a sink term of LBE volume fraction together with the corresponding sink term of energy localized on top of the riser and (ii) setting a source term of LBE volume fraction and energy with the same integral amount but localized at the top of the plenum. Due to the complex shape of the top plenum horizontal section, the source term covers the full LBE region over an horizontal slab, as shown in Figure 6, so that only a part of the subtracted LBE reappears in the plenum.

About 2% of the flowing LBE is transferred in this way. The effect is difficult to quantify because it depends on the temperature difference between the riser and the plenum top and should contribute to reduce this difference, though very slowly in time.

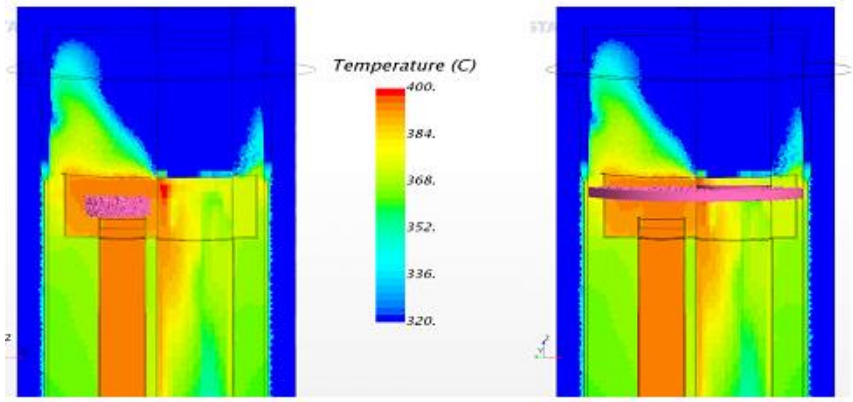

Figure 6: In pink, the localization of the sink (left) and source (right) terms.

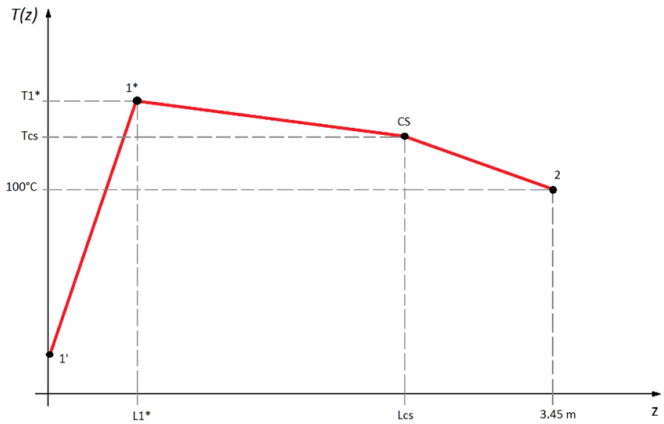

Figure 7: Heat exchanger secondary side temperature T_0 as function of height..

4.5 Heat Exchanger

As the secondary side tubes are not present in the model, cooling in the HX is obtained by setting there a sink term in the energy equation. The sink term has been constructed to be easily and understandably tuned for the purpose of the moment. The formula is the following:

$$Q_{HX} = \chi \cdot VF_{LBE} \cdot \frac{\rho c_p}{\tau}(T_0 - T), \qquad (5)$$

where χ is the support (localization) function and VF_{LBE} is the LBE volume fraction. All other parameters are similar to those of Equation (4). The main difference with that equation is the introduction of a support function. Formerly, it is implicitly represented through the application of the sink term to the dedicated numerical region. In the present case, by means of this support function, the sink term is applied to only a part of this numerical region. In fact, it is applied only to a hexagonal shape slightly smaller than the HX in an attempt to reproduce qualitatively what has been found through detailed CFD studies of the HX by itself; the LBE near the SGE wall is quite hotter than the mean on that level. Regarding T_0, it represents the secondary side's temperature. It varies as function of height in a similar way as in Figure 7, which is data coming from experiments.

Also, a porous medium approach is used to model the pressure losses due to the non-physically present tubes.

4.6 Conjugate Heat Transfer

As all structures are physically present in the model, including the correct wall thicknesses, conjugate heat transfer can take place in the model by thermally coupling these structures with the fluids they are in contact with.

5 NUMERICAL SETTINGS

To obtain the flow and temperature fields, the Navier-Stokes and energy equations are solved numerically in the RANS context. The corresponding settings for each model are summarized in Table 1. The turbulent Prandtl number is set to 2.0 according to Bricteux et al. (2012).

Table 1: Relevant simulation settings.

Settings	NRG's model	CRS4's model
CFD code	ANSYS Fluent 17.2	Star-CCM+
Turbulence model	Realizable κ-ε model	Realizable κ-ε model
Wall treatment option	Enhanced Wall Treatment	Two-layer all y+
Liquid metal heat transfer	Turbulent Prandtl number = 2.0	Turbulent Prandtl number = 2.0
Velocity-pressure coupling	SIMPLE algorithm	SIMPLE
Gradient discretization	Least squares cell based	Hybrid Gauss-LSQ
Spatial discretization	2nd order	2nd order
Linear system iterative method	Gauss-Seidel	AMG
Boundary conditions - flow	No-slip (except for free surface)	No-slip
Boundary conditions - temperature	Conjugate heat transfer	Conjugate heat transfer

6. RESULTS OF STEADY-STATE SIMULATIONS OF CIRCE-ICE

This chapter discusses results obtained from steady-state simulations performed with the two models presented in the Chapters 3 and 4. Table 2 summarizes the main experimental settings that serve as input for the two models. As can be seen, the experimental steady-states are different for the two models. Hence, results of the models are only compared with experimental data, i.e., no direct model-to-model comparison is done.

Table 2: Relevant reference experimental data used for steady-state simulations

Parameter	NRG's reference data	CRS4's reference data
FPS nominal power	~ 600 kW	~ 800 kW
LBE mass flow rate	60 – 70 kg/s	~ 65.6 kg/s
Average velocity in the FPS	~ 1m/s	~ 1m/s
HX thermal power removed	~ 500 kW	776 kW
DHR	inactive	inactive

6.1 Steady-State Results using NRG's CIRCE-ICE Model

Table 3 gives an overview of some relevant values of the simulation, along with the corresponding experimental values. As can be seen, there is some discrepancy between the power input in the simulations and in the experiment. A lower heat input in the model is used because some of the power supplied to the electrical cables in the experiment is lost due to Joule heating inside the Dead Volume [9]. This means less power is available for heating of the LBE. Heat removed by the heat exchanger in the model is very close to what is removed in the experiment. Also, the mass flow rate inside the inner loop agrees very well due to the tuning of the VMS in the riser.

The inlet and outlet temperatures of the inner loop, i.e., $T_{in,FPS}$ and $T_{out,HX}$ agree very well, with the former being almost exactly equal to the experimental value, while the latter is off by ~5°C. This is very important because it means that LBE flows out of and

into the main pool at approximately the correct temperatures. Other inner loop temperatures differ more, but are still reasonably close. The one outlier is the inlet temperature of the heat exchanger. This could be due to the measurement taken in a cold spot, as it is rather odd that temperatures suddenly drop by 13°C when exiting the riser and entering the heat exchanger, especially considering they are both at comparative levels.

Table 3: Steady-state conditions comparison between simulation and experiment.

	NRG's model	**Experiment**
Thermal Power in the FPS	550kW	600kW
ṁ LBE in the FPS	64.6 kg/s	~65 kg/s
ṁ LBE in the DHR	0.0 kg/s	0.0 kg/s
$T_{inlet,av}$ FPS	276.1°C	276.0°C
$T_{outlet,av}$ FPS (Fitting Volume)	335.8°C	334.2°C
$T_{inlet,av}$ Riser	332.3°C	329.2°C
$T_{outlet,av}$ Riser	330.0°C	331.2°C
$T_{inlet,av}$ HX	328.8°C	317.7°C
$T_{outlet,av}$ HX	271.9°C	267.0°C
$T_{inlet,av}$ DHR	319.3°C	318.7°C
$T_{outlet,av}$ DHR	278.4°C	280.3°C
$\dot{Q}_{water}$ removed by the HX	510kW	500 kW

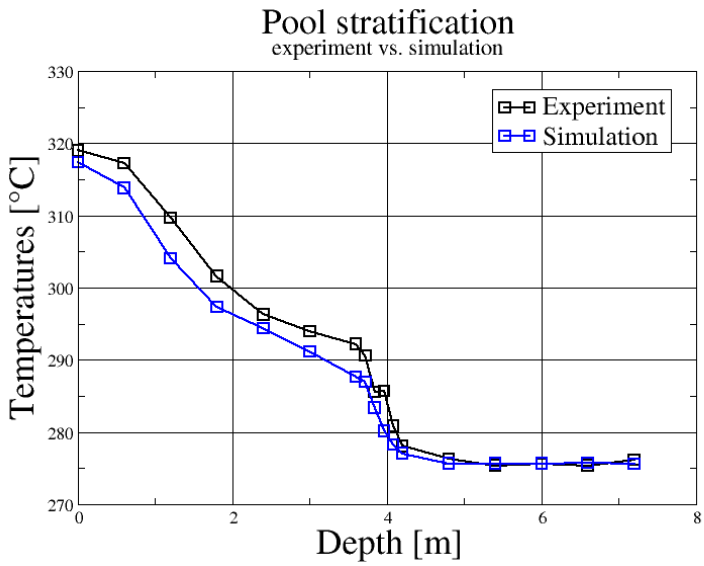

Figure 8: Stratification comparison inside the Main Pool.

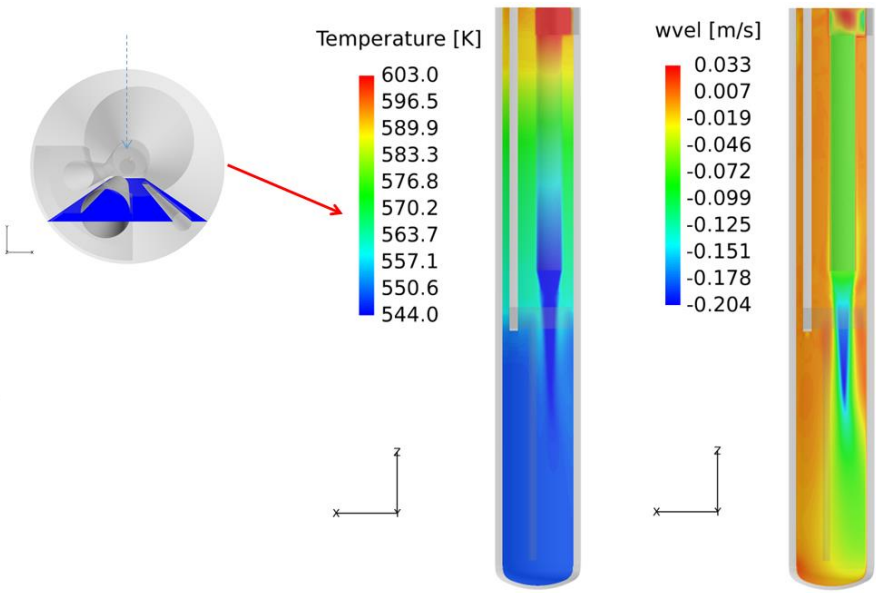

Figure 9: Temperature (middle) and vertical velocity (right) profiles on a vertical plane through the centre of the Heat Exchanger.

An important test of the model is how well the stratification of the Lead-Bismuth Eutectic inside the main pool is reproduced. This stratification is caused by heat losses from the inner loop, through the structure walls, to the main pool. Figure 8 shows a comparison between the simulations and experiment of the stratification for the steady-state flow. Here, a depth of 0m corresponds to the bottom of the separator and a depth of 7m to a level slightly below the inlet of the inner loop. Overall, a good agreement is found in the lower part of the vessel. The location of the steep temperature gradient around a depth of 4m, which corresponds to the fitting volume level, is properly captured. This steep temperature gradient is caused by large heat losses from the LBE inside the fitting volume, consisting of single-layered steel walls of about 10mm stick, to the main pool. In comparison, the FPS and riser are better insulated due to a double layer of steel with either air or stagnant LBE in between, resulting in much lower heat losses to the main pool.

Temperatures in the top of the pool are a couple of degrees lower in the model that in the experiment, indicating that probably more heat is lost through the riser and/or heat exchanger walls to the main pool in the experiment than is resolved by the model.

Some additional results of the model are shown in Figures 9 and 10, with the former showing temperature and vertical velocity profiles on a vertical cut through the main heat exchanger, and the latter showing temperature distributions on various vertical cuts through the system. Figure 10 shows that there is not much of a temperature variation on a horizontal plane; most differences occur vertically.

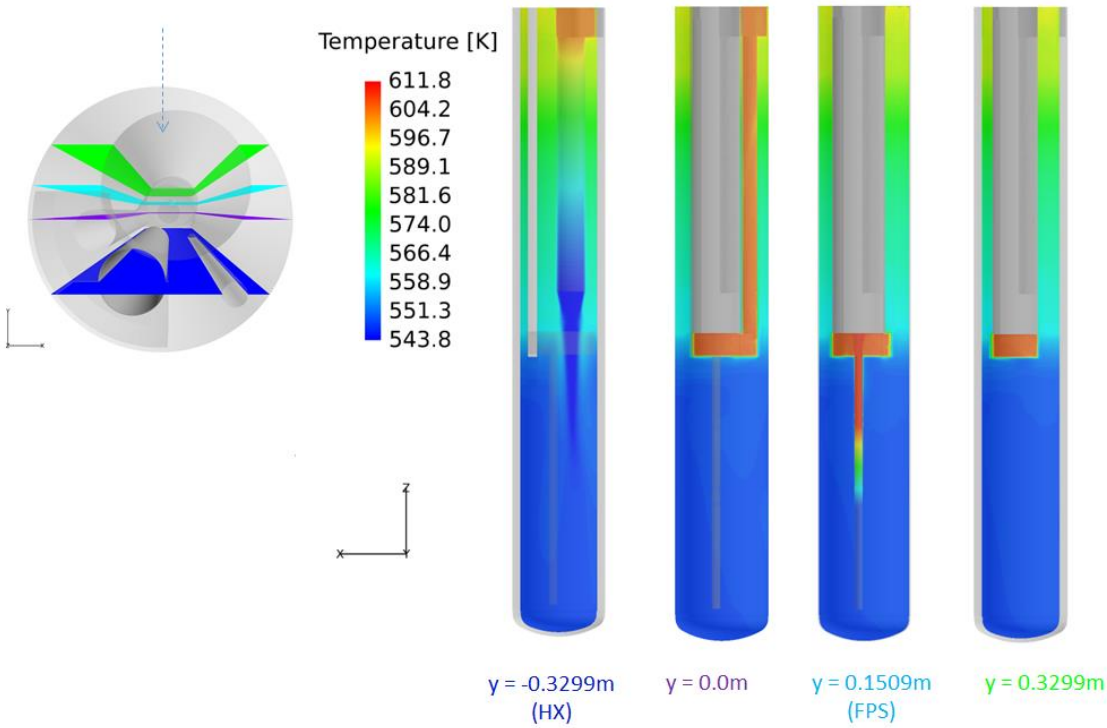

Figure 10: Vertical temperature profiles at, from left to right, y = -0.1509m (Heat Exchanger), y = 0.0m (centre Vessel), y = 0.1509m (FPS) and y = 0.3299m.

6.2 Steady-State Results using CRS4's CIRCE-ICE Model

In a pre-test phase of the model, quite large discrepancies were found between the model and experiments. This led to many improvements of the model, but also to a more thorough examination of the experimental data. It was found that the flow in the experiments is far less steady than anticipated and never really reaches thermal equilibrium. The mass flow rate in the FPS oscillates chaotically essentially between 63 and 69 kg/s and still varies between 65 and 67 kg/s when averaged over 60s. From the thermal point of view, the thermal imbalance is about 28kW during more than the last 3 hours of test. Moreover, the temperature probes at the heat exchanger bottom grid indicate a very uneven flow and cooling distribution and a complex time flow behaviour composed of a mix of slow variations, and some fast variations, these later appearing as jumps on the 10 hour time-scale. The flow below the heat exchanger bottom grid and around is also particularly unsteady, even at scales far beyond the turbulence ones.

These features bring intrinsic limitations to the validation of a steady-state numerical CFD representation. Moreover so because the numerical modelling makes use of unresolved regions: 1) the FPS and the HX because the pin and tube bundles are not geometrically represented and 2) the gas lift system in the riser and the flow separator is not represented by a bubbly flow but only through a lifting force density. In these regions, only integral or semi-integral values make sense. In particular, a comparison with the point wise values given by the thermocouples is of particular difficulty and must be considered as merely indicative.

In the end, only the plenum temperature data on the vertical thermocouple lines can be used for an experimental/numerical comparison. Trying to represent this vertical profile has been a large driving force between the modelling changes made to initial models and why so much detail is included in the geometry. It also prompted limiting the heat and cooling sources in the FPS and HX to numerical regions slightly smaller than their geometric shapes.

The main result is shown in Figure 11, which shows the numerical and experimental results of the plenum temperature vertical profile. The experimental results are shifted down by 15 K to allow a better comparison. The numerical profile now captures very well most of the characteristics of the experimental one, all changes of temperature gradient are qualitatively and quantitatively

captured. Only the total temperature drop between the intermediary and the bottom plateau is clearly overestimated numerically by about 11 K. The temperature drop from the top to the bottom of CIRCE is 61K experimentally and 72K numerically (18% more). The main causes are:

- 6% mass flow difference: 65.5 kg/s in experiment and 62 kg/s in the simulation.
- ~7% electric power difference: 800 kW is added in the model while in the experiment a part is lost in the dead volume.
- Experiment ~28 kW away from thermal equilibrium (3.5% of total heat source), and simulation only 10 kW away.

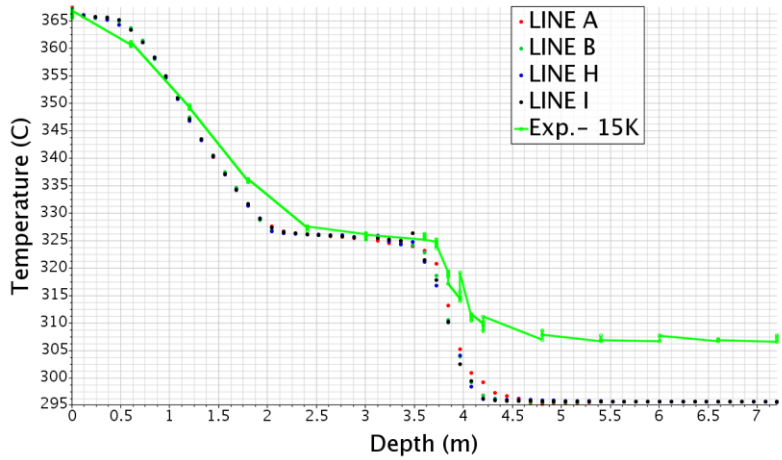

Figure11: Vertical temperature profiles of the numerical simulations (dots) compared with that of the experiment (green line).

From the numerical point of view, the flow in the plenum has become mostly coherent with two main coherent large structures below the HX outlet, as can be seen in Figure 12. Below the heat exchanger bottom grid, the cold flow forms a down-coming plume pushed away from the hot plume rising along the fitting volume. Some flow from the plenum enters the HX flow guide up to the lower grid. This feature is most probably unsteady and is the numerical counterpart of the high experimental variability. However, the strong coherence of the cold plume allowing it to better progress downward is probably the reason why mixing is limited below the HX in comparison with the experiment. In effect, from the experimental temperature measure below the HX, a much more complex and dispersive configuration is expected.

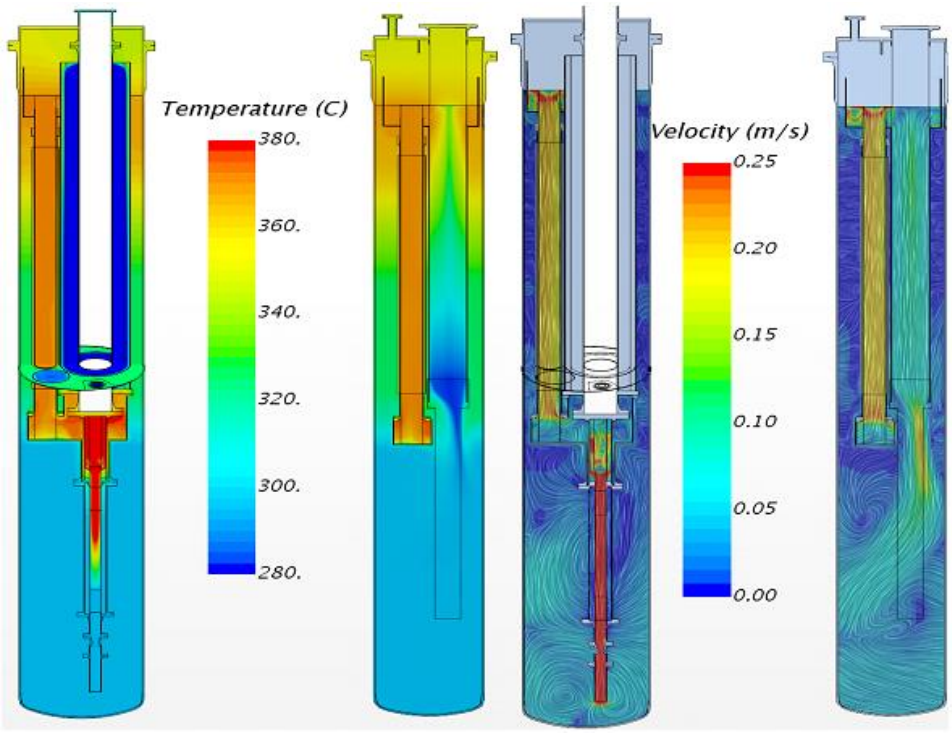

Figure12: Vertical planes crossing either FPS and riser or riser and HX. Left: temperature, right: velocity.

7. RESULTS OF NRG'S TRANSIENT SIMULATION OF CIRCE-ICE

Only NRG performed a simulation of a transient experiment, as CRS4 rather focussed their attention on refining their model to get better matching results for steady-state tests. The transient performed by NRG is SESAME WP3's Test 2. It consists of an initial

ramp-up to a steady-state flow with a total heat input of about 600kW and an LBE mass flow rate $\dot{m} = 60 - 70\ kg/s$. Furthermore, heat is removed by the main heat exchanger at a rate of 500 kJ per second. After having reached steady-state and running in steady-state for about 2.28 hrs, a Protected Loss Of Heat and Loss Of Flow (PLOH + LOW) accident scenario is mimicked. During such an accident scenario, the pumps stop working and the fuel operates at a decay heat, which is about 3-5% of its nominal power. Furthermore, the main heat exchanger is isolated from the system and the DHR serves as the heat sink of the system. In practise, the system goes from forced convection mode into natural convection at a much lower power. Figure 13 shows the power added to the system by the FPS on the left and the heat removed by the DHR on the right as function of time for the experiment.

To model the transition from forced to natural convection, the simulation is divided into two parts. The first 2.28 hrs represent the steady-state, forced convection, flow. It starts from when the simulation has reached a steady-state, so it does not represent or include the spin up from rest to the steady-state condition. This is actually the steady-state discussed in Section 6.1. After 2.28hrs, the simulation switches to transient conditions. The riser and heat exchanger are deactivated, the heat source in the FPS is set to 26kW and the DHR is turned on. The parameters of DHR model are set such that the total heat removed by the DHR during the simulation is about equal to that removed during the experiment.

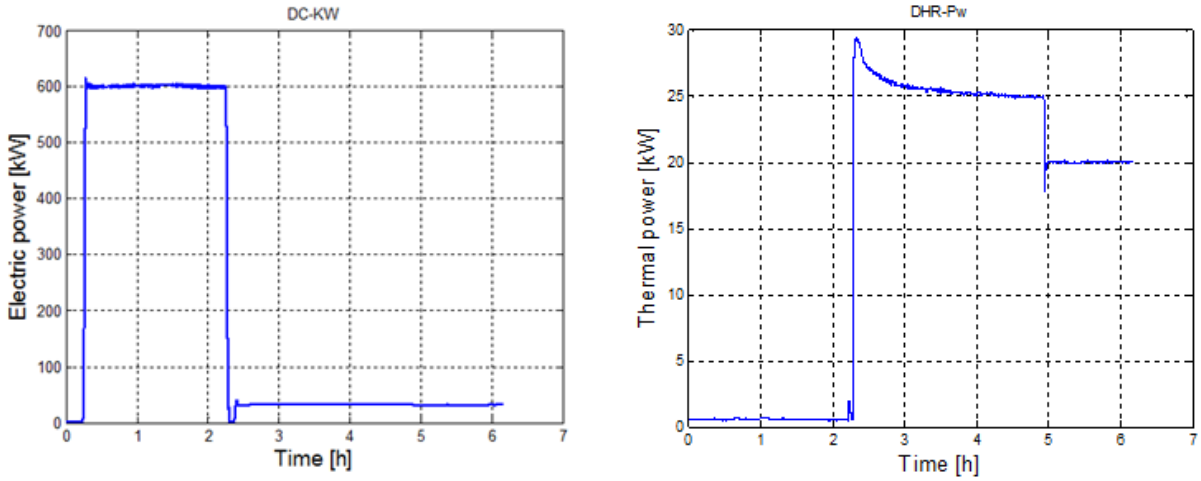

Figure 13: FPS input power and DHR heat removed as function of time for the experiment.

A comparison between the LBE mass flow rate in the inner loop for the experiment and numerical simulations is depicted in Figure 14. The general behaviour of the curve is well predicted in the simulation, especially considering that, during the transient part, the LBE circulates through natural convection, i.e., it is no longer an input but a result of the simulation. The undershoot is recovered by the model, though it takes longer before reaching the final steady state value.

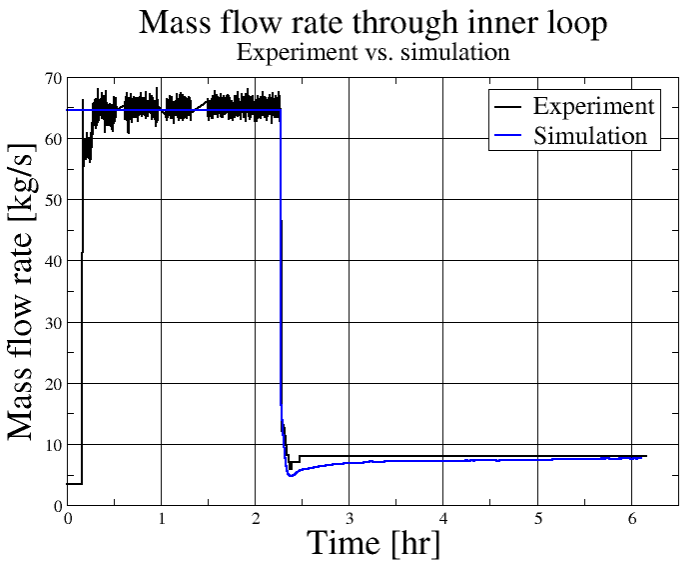

Figure 14: Mass flow rate through the inner loop as function of time.

Figure 15 shows the inlet and outlet temperatures of the FPS, on the left, and HX, on the right, for both the experiment and the numerical simulations. The initial flat temperatures found in the CFD analyses (from t = 0hrs to t = 2.28hrs), are due to the fact that, as mentioned before, the simulation does not include the start up from rest but has constant conditions throughout the steady-state part. Regarding the FPS, the inlet temperature agrees nearly perfectly with that of the experiment, especially in the last two hours of the transient. The outlet temperature is a couple of degrees higher in the numerical model, though it is still decreasing and may eventually settle to a value very close to that of the experiment.

As for the heat exchanger, the profiles of both temperatures agree reasonably with those of the experiment; the inlet temperature shows an initial strong drop followed by a slower decrease, while the outlet temperature initially increases and subsequently decreases. The final temperatures of the model are very close to those of the experiment, though the simulation shows some steady decrease in temperature still, while in the experiment they are closer to having reached a stable value. These temperature profiles indicate that the model cools off slower than the experiment.

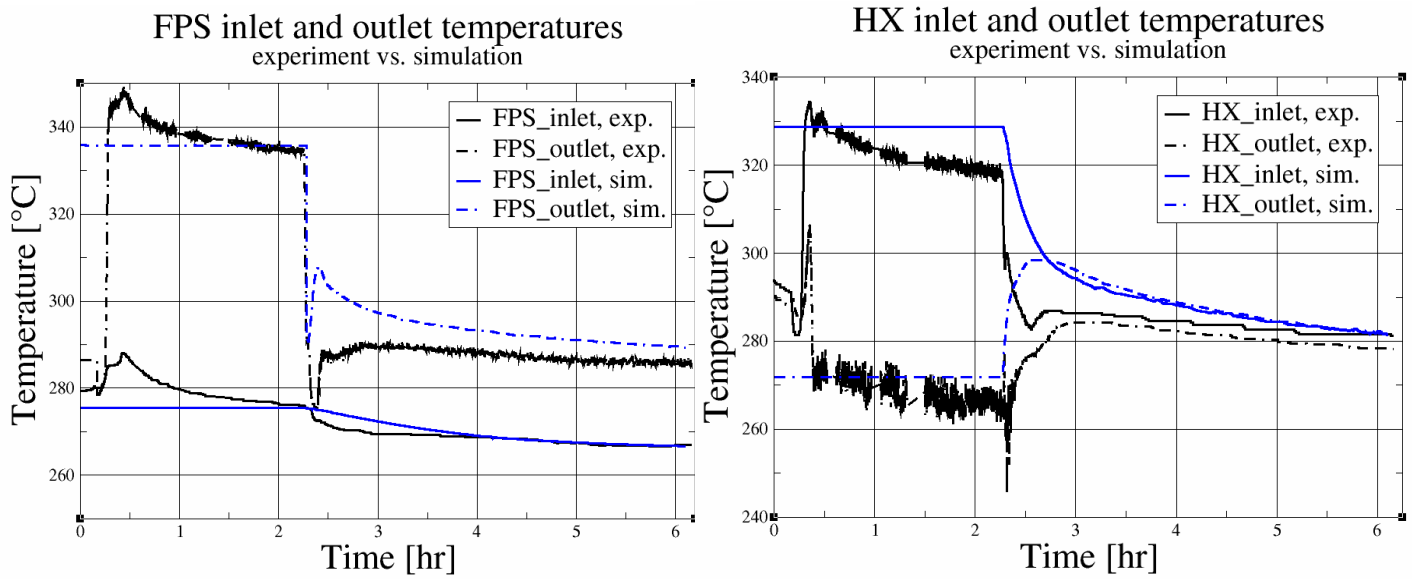

Figure 15: Inlet and outlet temperatures of the FPS (left) and HX (right) of the experiment and simulation.

Finally, a comparison of the stratification in the main pool between the experiment and numerical findings is presented in Figure 16. The best agreement between the two profiles is found at the end of the test, after 6.1hrs, when the stratification resolved by the simulation is nearly equal to that resulting from the experiment. This indicates that during the transient part of the simulation, the total amount of heat removed by the DHR is very close to that of the experiment. This is a good result, as this was used, among others, as input to calculate the parameters of the DHR's heat sink model. At the other two instances, the temperature profiles in the main pool of the experiment are below those of the model, indicating again that stronger cooling occurs in the experiment for the first part of the test than what is found in the simulation. At t = 4.5hrs, the temperature in the bottom of the pool already agrees between the experiment and the simulation though, as well as the location of the stratification inside the pool. Only the temperature of the top part is lagging behind.

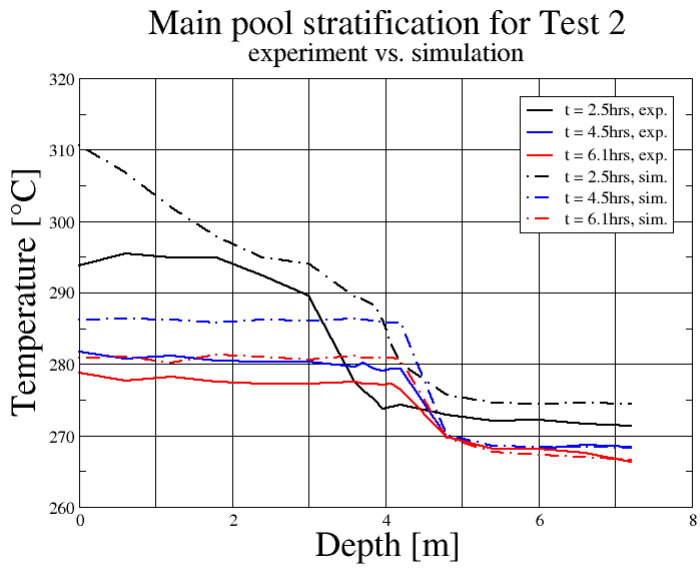

Figure 16: Comparison between the experiment and simulation of the stratification inside the main pool at three different times.

8. RESULTS OF STEADY-STATE SIMULATIONS OF CIRCE-HERO

Following the considerations presented in the previous chapters regarding the CIRCE-ICE design, a CFD model for the CIRCE thermal loop facility with the HERO heat exchanger configuration is created. HERO is a much longer (~ 7 m) and thinner heat exchanger than the CIRCE-HX, having only seven bayonet tubes. It is better insulated than the ICE HX and is encapsulated in an hexagonal matrix which does not let large border volumes without cooling. The CIRCE-HERO models takes profit of the lessons learned from the two previous ones (see Chapters 3, 4, 6 and 7). The bayonet tubes are again not included in the model.

This chapter discusses the main results obtained from steady-state simulations. A test reference case, defined in Lorusso et al. (2018), has been adopted by NRG, while different operating conditions, taken from (Rozzia 2016-1), have been used by CRS4, see Table 4. The power used in CRS4's model is much higher than the reference case, resulting, as can be seen later, in a much more pronounced stratification It must be noted that experimental results are available for the reference case only. This means that NRG's results are compared to experimental findings, while CRS4's results will be shown without comparison to actual CIRCE-HERO experiments.

Table 4: Relevant reference experimental data used for steady-state simulations of CIRCE-HERO

Parameter	Lorusso et al. (2018) and NRG	CRS4
FPS nominal power	~ 90 kW	450 kW
LBE mass flow rate	~ 30 kg/s	44.7 kg/s
HX thermal power removed	~ 77 kW	~ 428 kW
DHR	removed	removed

8.1 Steady-State Results using NRG's CIRCE-HERO Model

As done for the ICE configuration, an overview of some relevant values of the simulation, along with the corresponding experimental values, is presented in Table 5. Very good comparisons can be observed for all the quantities investigated. The only exception is the temperature at the outlet of the riser. In the CFD, it is lower than the riser inlet temperature, due to heat transfer from the riser to the pool. However, in the experiments the riser outlet temperature is higher than the riser inlet temperature. This can be explained by looking at the temperature contours and the stratification profiles presented below. In particular, the upper part of the facility seems to be at a high temperature in the experiments, with no stratification present until reaching almost the outlet of the HERO HX, as evident in the stratification plot shown in Figure 17. Compared to the ICE configuration, additional thermocouples have been included in the experiments to try to capture correctly the stratification in HERO, since the stratification level appears at a different height. However, the radial location of the thermocouples is the same as for CIRCE-ICE. Similarly, the same reference is used for the depth of the pool, i.e. a depth of 0 m corresponds to the bottom of the separator and a depth of 7 m to a level slightly below the inlet of the inner loop. Overall, a good agreement is found in terms of temperature difference between the upper part and the bottom part of the pool, as confirmed by the comparison presented in Table 5. However, it is evident how the CFD calculations predict a higher stratification, around 3-4 m, while in the experiments the stratification appears around 5 m.

Table 5: Steady-state conditions comparison between simulation and experiment.

	NRG's model	Experiment
Thermal Power in the FPS	87.4 kW	90 kW
ṁ LBE in the FPS	30 kg/s	~30 kg/s
$T_{inlet,av}$ FPS	221.3°C	~220-221°C
$T_{outlet,av}$ FPS (Fitting Volume)	241.7°C	~240-241°C
$T_{inlet,av}$ Riser	239.9°C	~239-240°C
$T_{outlet,av}$ Riser	238.2°C	~240-241°C
$T_{inlet,av}$ HX	238.1°C	~239°C
$T_{outlet,av}$ HX	220.3°C	~222°C
$\dot{Q}_{water}$ removed by the HX	76.1 kW	77 kW

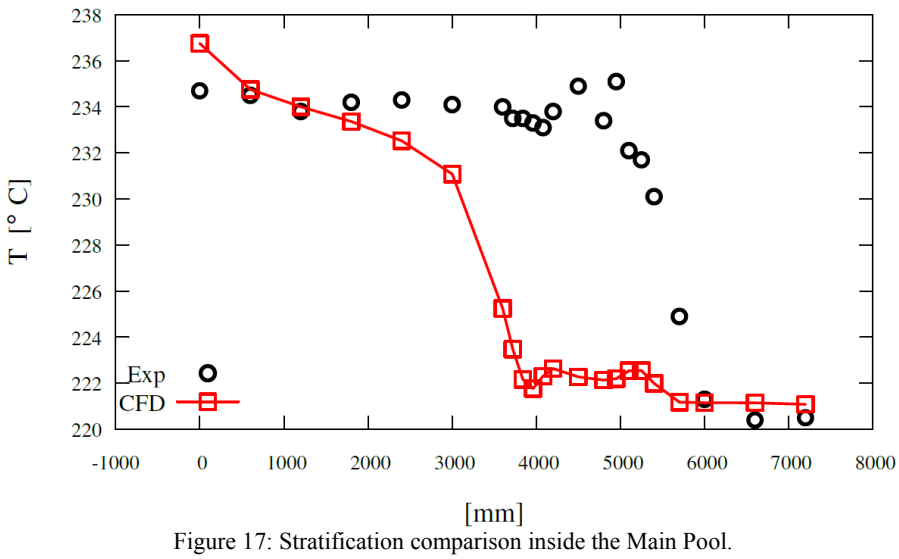

Figure 17: Stratification comparison inside the Main Pool.

Consistent with the CIRCE-ICE scenarios, contours of temperature and vertical velocity on a vertical cut through the main heat exchanger and contours of temperature on various vertical cuts through the facility are presented in Figs. 18 and 19. It is evident in these contours that stratification is mainly vertical and develops in correspondence of the fitting volume. Furthermore, the velocity is different compared to the CIRCE-ICE configuration, since the HX is longer here, causing a mixing at a lower level in the pool.

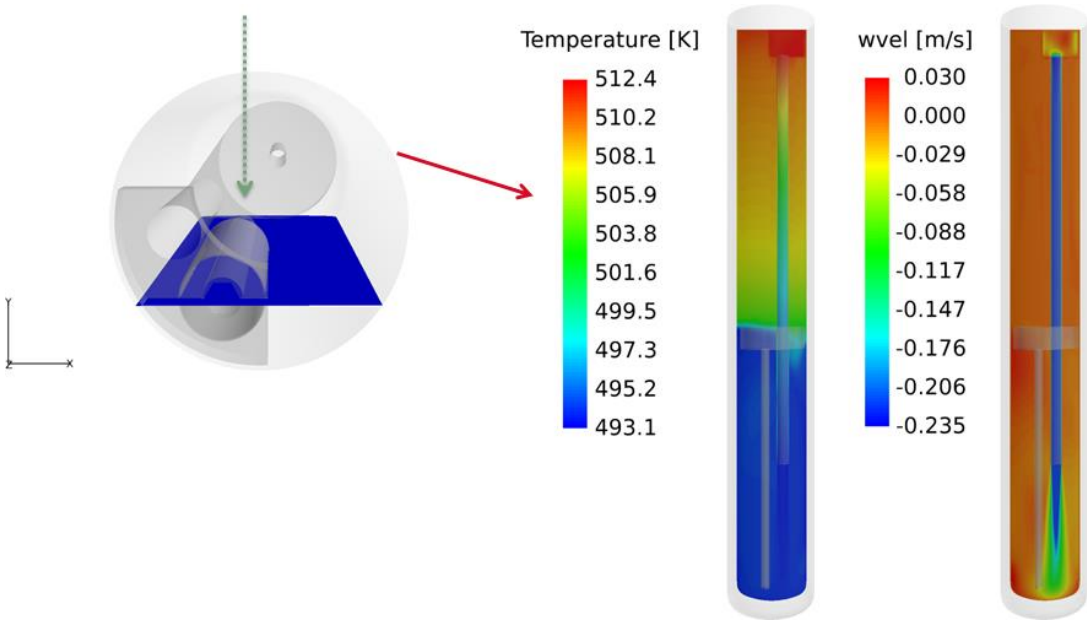

Figure 18: Temperature (middle) and vertical velocity (right) profiles on a vertical plane through the centre of the Heat Exchanger.

The discrepancy in the stratification level has been investigated in detail and it has been noticed that in the CFD calculations the stratification location evolves from values close to the experiments and reaches the final level presented in Fig. 17. For this reason, a transient calculation was also carried out to further analyse the evolution of the stratification level. As can be seen in Fig. 20, after 500 s the pool stratification appears around 5m, consistent with the experimental findings. However, as time passes, the stratification level moves up (towards lower depths), suggesting some uncertainties in the time constant, since the pool seems to get colder faster than in the experiments. Another reason might be the uncertainties in the heat capacities of the different components. It must be noted here that for the internal walls the same conditions as for CIRCE-ICE are adopted, while for the external vessel a convective boundary condition is used, with a constant value of the heat transfer coefficient equal to 2 W/(m^2 ·K). This value is based on the characterization of heat losses in the experiments provided by Pesetti et al. (2018b), but it might be a source of uncertainty that should be further investigated.

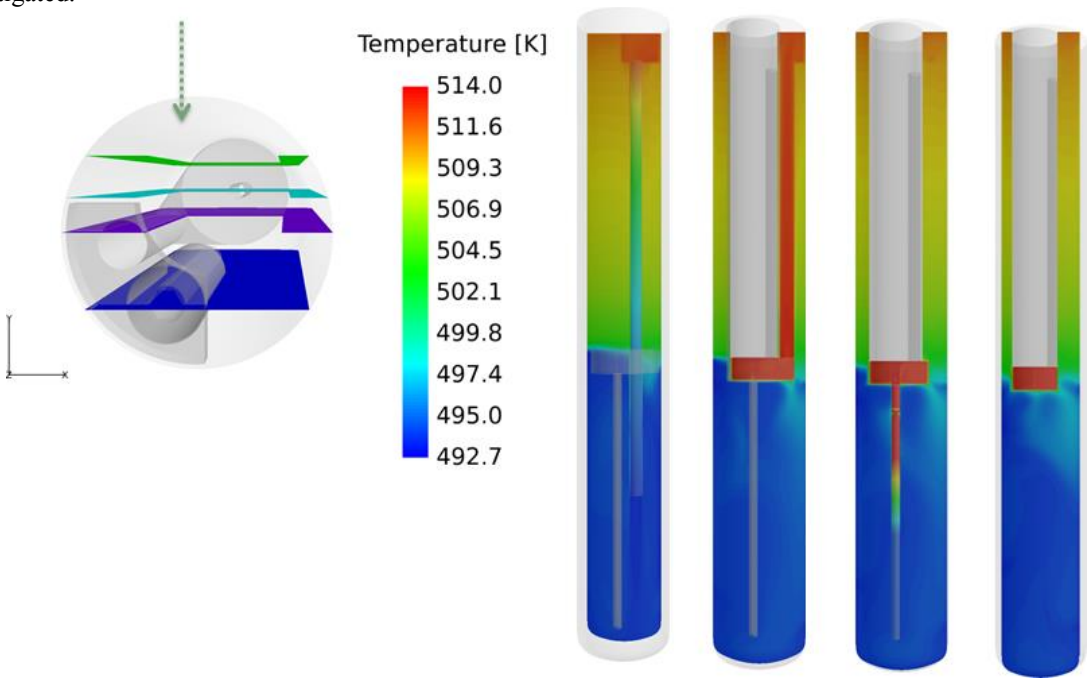

Figure 19: Vertical temperature profiles at, from left to right, y = -0.1509m (Heat Exchanger), y = 0.0m (centre Vessel), y = 0.1509m (FPS) and y = 0.3299m.

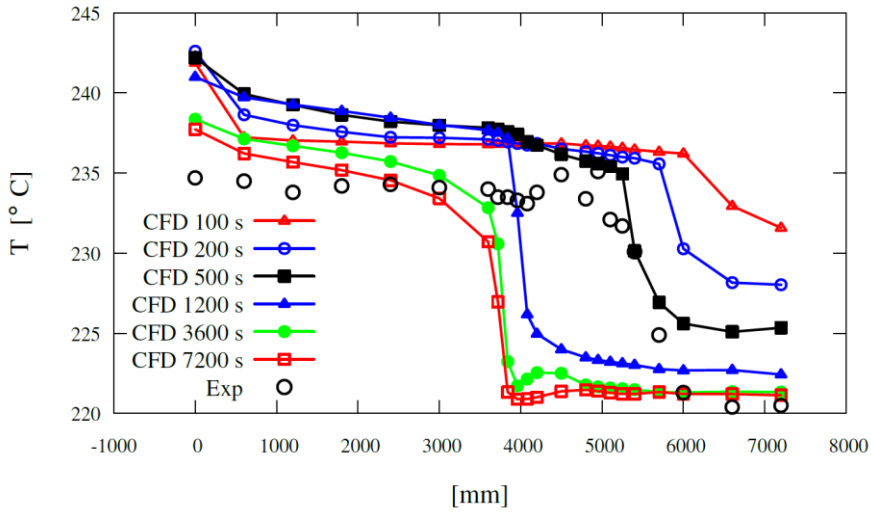

Figure 20: Stratification evolution inside the Main Pool at different times for the unsteady calculation.

8.2 Steady-State Results using CRS4's CIRCE-HERO Model

The present model is updated and adapted from a pre-existing model developed in the framework of the SESAME project. The numerical model was initially developed for the ICE configuration and operated by CRS4 within the VoF framework. Because there are no significant changes of free surface levels and there was an issue with the LBE behaviour in the stagnant part of the plenum, it was decided to build a new CFD model but with sufficient modularity to be operated either in single phase flow or with the VoF setting from one part and to be also easily adapted to the HERO configuration. Steady state numerical simulations for the conditions presented in Table 4 are presented here. The vertical profile of temperature is given on four chosen positions in correspondence to four TC lines defined in Pesetti et al. (2018a). It is composed of two plateaus, a hot one above 450 C above depth 4m and a cold one at 400 C below depth 5m. A sharp thermal transition about 1m high but with a 40cm very high gradient (range 4.4-4.8m) lies in between, see Figure 21 This thermal profile is highly different from a typical experimental test case in ICE configuration, also shown on the same figure for comparison. Even though the conditions are different from the CIRCE-HERO test reference case, it is interesting to note that the stratification location predicted by the CRS4 model is also higher than the one observed in the experiments (see Fig. 17). Future application of the CRS4 model to the reference test case might bring more insights about these discrepancies.
.

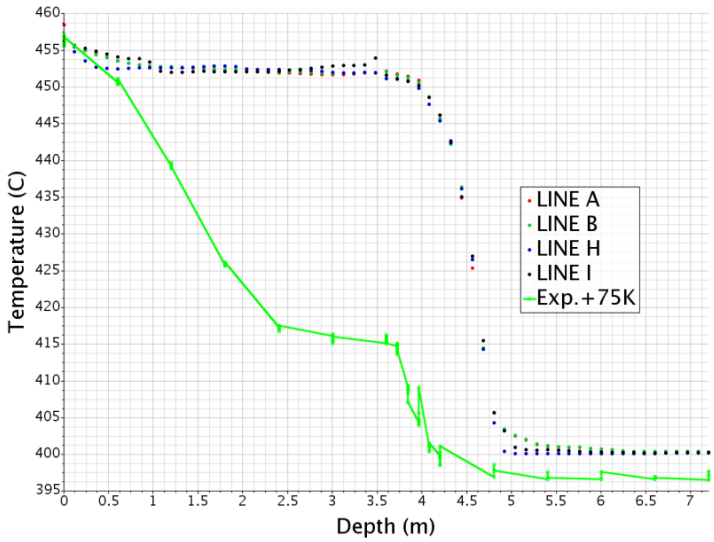

Figure 21: temperatures along 4 TC lines (dots) and rescaled experimental temperatures in an ICE test case.

9. CONCLUSIONS

The present paper describes CFD models created by NRG and CRS4 of the CIRCE facility. This facility initially was furbished with a 91 bayonet tube heat exchanger and a designated decay heat removal system, the ICE configuration. Experiments in this configuration were performed as part of the H2020 projects SESAME and MYRTE. During these same projects, the heat exchanger was replaced by another one named HERO, which also serves as DHR in accident scenarios, and another series of experiments were done with this new set up. The purpose of these experiments was twofold: 1) provide data for liquid metal fast reactor designs and 2) generate a database to validate CFD models with. The current papers focusses on the second part.

The CFD models of CIRCE-ICE created by both partners reproduce the general flow and temperature patterns of the facility operating under nominal and transient conditions quite well. However, some discrepancies are found as well, most noteworthy for

the pool stratification. After some investigation, it was discovered that this stratification is quite sensitive on the modelling of the conjugate heat transfer from the inner loop to the pool. Improvements were made to this respect, resulting in a better match with experimental data. CRS4 found some other potential explanations of the encountered differences in results between model and experiment, such as the existence of a bypass flow. Overall, modelling results of CIRCE-ICE served as valuable feedback to the experimentalist, resulting in changes made to the facility and a better data acquisition.

Lessons learned from the modelling of CIRCE-ICE were, as far as possible, applied to the modelling of CIRCE-HERO. Similar observations as for CIRCE-ICE can be made; the inner loop temperatures match quite well, though the stratification inside the plenum requires further research.

ACKNOWLEDGMENT

The authors would like to thanks the European Commission for its financial support within the HORIZON2020 SESAME program (n^0 654935).

NOMENCLATURE

Symbol	Quantity	SI Unit
A	Surface area	m^2
C_2	Inertial resistance coefficient	1/m
c_p	Specific heat	J/(kg·K)
L	Length	m
$\dot{m}$	Mass flow rate	kg/s
P	Power	W
p	Pressure	Pa
Q	Volumetric heat source/sink	W/m^3
S	Momentum source	$kg/(m^2 \cdot s^2)$
T	Temperature	K
V	Volume	m^3
v	Velocity	m/s
α	Permeability	m^2
μ	Dynamic viscosity	Pa·s
ν	Kinematic viscosity	m^2/s
ρ	Density	kg/m^3
τ	Relaxation time	s
χ	Volume fraction	-

REFERENCES

Bandini, G., Di Piazza, I., Gaggini, P., Del Nevo., A., and Tarantino, M., 2011. CIRCE experimental set-up design and test matrix definition. ENEA UTIS-TIC Technical Report, IT-F-S-001.

Bricteux, L., Duponcheel, M., Winckelmans, G., Tiselj, I., and Bartosiewicz, Y. 2012. Direct and large eddy simulation of turbulent heat transfer at very low Prandtl number: Application to lead-bismuth flows. Nuclear Engineering and Design, vol. 246, pp.. 91-97.

Lorusso, P., Pesetti, Polazzi, G., Sermenghi, V. and Tarantino, M., 2018. CIRCE EXPERIMENTAL REPORT. Report ENEA CI-I-R-353.

Pesetti, A., Forgione N., Narcisi, V., Lorusso, P., Giannetti, F., Tarantino, M., and Del Nevo, A., 2018a. ENEA CIRCE-HERO Test Facility: Geometry and Instrumentation Description. Report ENEA CI-I-R-343.

Pesetti, A., Polazzi G., Sermenghi, V. and Tarantino, M., 2018b. ENEA CIRCE-HERO Test Facility: Heat Losses Characterization. Report ENEA CI-I-R-351.

Rozzia, D., Del Nevo A., Tarantino M., and, Giannetti F., SESAME deliverable D4.3 – CIRCE-HERO test setup, issued on 04/04/2016 by ENEA.

Rozzia, D., Del Nevo, A. and Tarantino, M., 2016. Experimental Investigation of Double Wall Bayonet Tubes Performance in Pool Type Integral Test Facility, 16th International Meeting on Nuclear Reactor Thermal Hydraulics (NURETH-16), Chicago, US, August 30-September 4 2016, American Nuclear Society.

Tarantino, M., Scaddozzo, G., 2006. Test specifications of the Integral Circulation Experiments. Report ENEA ET-F-S-001, Deliverable D.4.15, DM4 DEMETRA, IP-EUROTRANS.

Tarantino, M., 2013. CIRCE Experimental Report. THINS deliverable D2.1.06.

Tarantino, M., Martelli., D., Barone., G., Di Piazza, I., and Forgione, N., 2015. Mixed convection and stratification phenomena in a heavy liquid metal pool. Nuclear Engineering and Design, vol. 286, pp. 261-277.

Todreas, N.E., and Kazimi, M.S., 1993. Nuclear System I, Thermal Hydraulic Fundamentals. Taylor & Francis.